Proceedings World Geothermal Congress 2020+1
Reykjavik, Iceland, April - October 2021

A Numerical Study On The Potential Of Seismic Body Waves To Initiate Colloidal Mobilization In Fluid-Saturated Fractured Rocks

Nicolás D. Barbosa (UNIGE), Simón Lissa (UNIL) and Matteo Lupi (UNIGE)

Department of Earth Sciences, University of Geneva, Rue des Maraîchers 13, 1205, Geneva, Switzerland

nicolas.barbosa@unige.ch

Keywords: Fracture unclogging, permeability enhancement, dynamic triggering, seismic stimulation

ABSTRACT

Dynamic stresses imposed by the waves of distant earthquakes are known to trigger numerous hydrological phenomena in the upper crust. Many laboratory and field studies have shown that fracture permeability enhancement due to seismically-induced colloidal mobilization at the fracture scale can produce pore fluid pressure redistribution at the reservoir scale. Geothermal systems are particularly susceptible to this mechanism due to the constant precipitation of minerals and sediments from geothermal fluids that eventually leads to the clogging of open fractures. In this scenario, fracture unclogging has been evoked to explain the pore fluid pressure redistribution that can lead to frictional instabilities and seismicity as well as a phenomenon inhibiting the formation of obstacles to fluid flow in regions with frequent seismic activity. The evidence suggests that seismically-induced viscous shear stresses in the fluid saturating a fracture in the range of tenths of Pascals is sufficient to initiate colloidal mobilization. In this work, we numerically assess the development of viscous shear stress in the fluid saturating a system of fractures due to the action of seismic body waves. We perform a sensitivity analysis of the wave-induced viscous shear stresses in terms of fluid, fracture, and background rock physical properties as well as seismic wave characteristics. Our results show that seismically induced viscous shearing in the order of those initiating fracture unclogging are plausible for typical seismic strains. For an anisotropic distribution of fractures, viscous shearing increases with frequency and the imposed seismic strain and is extremely dependent on the mode and direction of wave propagation. This implies that, for seismic waves of similar strain amplitudes and frequencies, directivity is a key factor controlling the occurrence of dynamic triggering events. For similar seismic wave characteristics, larger viscous shearing is expected for more viscous fluids, stiffer background rock, and thinner fractures. The latter is particularly important as we found that spatially heterogeneous fracture apertures can produce locally enhanced viscous shear stress. This points out that regions where pore fluids conditions change or with different fracture properties may be more sensitive to fracture unclogging, and consequently permeability enhancement, than others.

1. INTRODUCTION

The mechanical and hydraulic properties of reservoirs are very sensitive to the presence of open fractures. In the particular case of geothermal reservoir characterization, the critical role of open fractures on fluid transport may determine whether geothermal reservoirs are economically exploitable or not. Hydraulic stimulation is arguably the most effective method to increase the hydraulic conductivity of a reservoir through the creation of new conductive fractures (Economides and Nolte, 1989). However, the hydraulic conductivity of fractures is a transient property (e.g., Borg et al., 1976; Ameli et al., 2014; Pyrak-Nolte and Nolte, 2016). For example, when a colloidal particle travels through a fluid-saturated fracture, it is affected by several processes that promote their attachment to the fracture wall ultimately reducing the hydraulic conductivity of the fracture in a process commonly referred to as fracture clogging. Geothermal systems are particularly susceptible to this mechanism due to the circulation of minerals and sediments present in the geothermal fluids that eventually leads to the clogging of open fractures. On the other hand, when hydrodynamic drag forces in the fluid of the fractures overcome the adhesive forces, colloidal detachment from fracture surfaces or "fracture unclogging" can be initiated (Bergendahl & Grasso, 2000). In this scenario, instead of creating new fractures, the overall permeability of the reservoir is increased by the mobilization of colloids at the pore scale through pre-existing fractures (Elkhoury et al., 2011).

The dynamic shaking associated with the seismic waves from earthquakes is a natural source of hydrodynamic drag forces in the fluid saturating open fractures. Indeed, seismically-induced fracture unclogging has been recognized as a mechanism of permeability enhancement that could explain a number of hydrological and hydrogeological responses to distant earthquakes (Rojstaczer et al., 1995, Manga et al. 2012). Field observations at the regional scale showed that passing seismic waves affected stream-flow and spring discharge (e.g., Manga et al., 2003), groundwater level (e.g., Brodsky et al., 2003; Elkhoury et al., 2006; Kocharyan et al., 2011; Xue et al., 2013; Y. Zhang et al., 2015), oil wells production (Beresnev and Johnson, 1994; Mirzaei-Paiaman and Nourani, 2012), temperature and composition of groundwater (Mogi et al., 1989). Permeability increases promoted by passing seismic waves are particularly effective in geological systems characterized by elevated pore pressures at depth (Manga and Brodsky, 2006; Farías et al., 2014). This is the case in geothermal systems or in geological settings where isolated compartments of high pressure fluids may develop at depth. The subsequent redistribution of the pore fluid pressure may, in turn, cause seismicity at geothermal systems (Lupi et al., 2017), eruption of mud volcanoes (Rudolph and Manga, 2010; Lupi et al., 2013), and liquefaction of unconsolidated sediments (Wang, 2007). Although dynamic triggering effects are typically associated with the seismic energy of surface waves generated by teleseismic events (Brodsky et al., 2003; Brodsky & Prejean, 2005; Elkhoury et al., 2011), it has been shown that body waves released from regional earthquakes can have a similar impact on a variety of fluid-saturated systems (Lupi et al., 2013, 2015; Lupi et al., 2017). The effects of body waves can be even more important than those related to surface waves in geological settings (e.g. anticlines) focusing and amplifying the incoming seismic energy (Lupi et al., 2017).

Based on the documented field evidence and subsequent laboratory experiments, the implementation of seismic sources has been suggested as a cost effective permeability enhancement method in geothermal systems, where permeability is primarily related to

open fractures. Indeed, the use of stimulation through the application of dynamic shaking has been suggested and tested as a low-cost and environmentally friendly enhanced oil recovery method (Beresnev and Johnson, 1994). In that case, downhole seismic sources in stimulation wells are used to create seismic waves by a sudden release of fluid inside the borehole, which, in turn, increase oil mobility (e.g., Pride et al., 2008). Despite the engineering challenge that artificial stimulation of reservoirs represent, to date, the underlying physics of seismically-induced fracture unclogging are still not well understood. In this work, we propose a methodology to compute the transient drag forces created by passing seismic waves in the fluid saturating a system of fractures. In particular, we examine whether body waves could sufficiently stimulate a fractured formation to initiate the fracture unclogging.

2. METHODOLOGY

Experimental and theoretical studies (Bai and Tien, 1997; Bergendahl and Grasso, 2000; Brodsky et al., 2003; Kutay and Aydilek, 2009; Li et al., 2005) have shown that colloidal detachment from the surface of poroelastic materials is positively correlated with the development of strong viscous shear stresses in the pore fluid of the porous medium. Hence, a first step to understand permeability changes driven by colloidal mobilization in fluid-saturated fractured rocks is to investigate how such drag forces are created in response to seismically-induced pore pressure oscillations. In general, the viscous shear stress tensor components τ_{ij}, caused by the motion of a viscous fluid are defined as (Kutay and Aydilek, 2009)

$$\tau_{ij} = \eta\left(\frac{\partial v_i}{\partial x_j} + \frac{\partial v_j}{\partial x_i}\right), \qquad i,j = x,y,z, \tag{1}$$

where η is the fluid viscosity and v_j is the j-component of the fluid velocity. Eq. 1 links the velocity gradients generated due to the presence of local pressure gradients with the magnitude of the viscous shear stress acting on the fluid-solid interface. Manga et al. (2012) related observations of colloidal mobilization in a wide range of systems to an estimation of the viscous shear stress that is transiently applied to the colloids. They found that relatively low viscous shear stresses in the order of 0.1-1 Pa appear to be sufficient to produce measurable evidence of colloidal mobilization.

In the case of seismically-induced fracture unclogging, the viscous shearing (Eq. 1) is caused by the shaking imposed by seismic waves whose wavelengths are typically much larger than the fractures (Brodsky et al., 2003). In order to bridge such a scale gap in a numerically efficient way, we emulate the action of a propagating seismic wave directly at the scale of a representative elementary volume (REV) that is structurally and seismically typical of the whole fractured formation of interest and much smaller than the dominant seismic wavelengths. This is achieved by applying a set of oscillatory displacement fields on the boundaries of an REV of the fractured formation of interest (Fig. 1 arrow a and Fig. 2). This numerical approach allows us to focus on sub-wavelength scale features and processes, such as, viscous shear stresses in the fractures, that occur in response to the seismic strains associated with seismic waves (Fig. 1 arrow b).

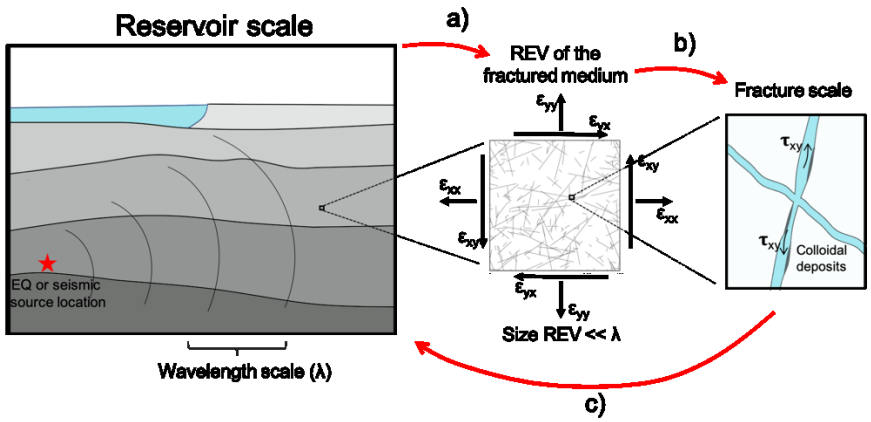

Figure 1: Schematic illustration of the methodology used to compute seismically-induced viscous shear stresses at the fracture scale. A propagating body wave imposes transient strains to a fractured formation of interest, which we emulate by applying an oscillatory relaxation test to the REV of the formation (a). The imposed strains produce pressure gradients and fluid motion inside the fractures, which create viscous shear stresses (b). The viscous shearing applied to colloidal deposits can detach them from the fracture walls leading to changes in the overall hydraulic conductivity of the formation (c).

The mechanism of creation of seismically-induced viscous shear stresses in the fluid saturating a fractured formation can be explained as follows. When the passing body waves compress the fracture formation, fluid pressure gradients are created between the fractures and the background rock and also between hydraulically connected fractures. During the corresponding fluid pressure equilibration, seismic energy is dissipated, which is commonly observed in the form of seismic attenuation and velocity dispersion (Rubino et al., 2013). In this work, we assume the background rock to have very low porosity and permeability and neglect the fluid pressure diffusion (FPD) process between the fractures and the background. Instead, we explore the link between the seismically-induced FPD between connected fractures (briefly FF-FPD) and the development of viscous shear stresses at the walls of the fractures (Fig. 1 arrow b). We refer the reader to the work of Quintal et al. (2016) for a detail explanation of the numerical solution of the system of equations coupling the laminar flow of a compressible viscous fluid in the fractures (quasi-static linearized Navier-Stokes equation) with the elastic deformation of the background rock (linear elastic equation for a nonporous solid material). This methodology allows for modelling the associated spatial flow patterns inside the fractures (Quintal et al., 2016) from which the viscous shear stress can be obtained using Eq. 1 and also the associated frequency-dependent seismic wave attenuation and velocity dispersion.

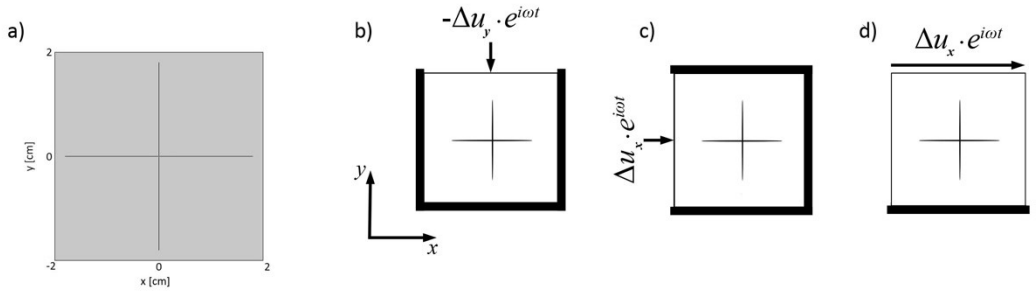

Figure 2: a) Synthetic sample representing a unit cell of a periodically fractured rock containing two connected orthogonal fluid-saturated fractures. The background is assumed to be elastic and the fractures are saturated with a viscous fluid. Panels b), c), and d) show the imposed boundary conditions for the vertical, horizontal, and shear relaxation tests, respectively. Vertical and horizontal relaxation tests simulate the action of a normally (perpendicular to the *x*-axis) and horizontally (parallel to the *x*-axis) incident P-wave. The shear relaxation test simulates the action of normally incident S-wave.

For the computation of the seismically-induced viscous shear stress in the fluid of the fractures, we first consider a 2D numerical model corresponding to an REV of a periodically fractured medium (Fig. 2). The 2D problem that we tackle is equivalent to a 3D case where the strains outside the modelling plane are zero. We refer as x and y to the orthogonal directions in the modelling plane (Fig. 2) while z is the direction perpendicular to the x-y plane. In this case, the only non-zero component of the viscous shear stress tensor shown in Eq. 1 is τ_{xy}. At a given position inside the REV, the component τ_{xy} resulting from an arbitrarily imposed strain state can be computed as (Rubino et al., 2016)

$$\tau_{xy}^{\varepsilon} = \varepsilon_{xx}\tau_{xy}^{11} + \varepsilon_{yy}\tau_{xy}^{22} + \varepsilon_{xy}\tau_{xy}^{12}, \tag{2}$$

where the strain state imposed to the sample is defined by the components ε_{xx}, ε_{yy}, and ε_{xy}. τ_{xy}^{11}, τ_{xy}^{22}, and τ_{xy}^{12} are the viscous shear stresses in response to strain states that have $<\varepsilon_{xx}>=1$, $<\varepsilon_{yy}>=1$, $<\varepsilon_{xy}>=1$, respectively, while the rest of the strain components are zero. Although not shown for brevity, it is straightforward to obtain those fields using the responses to the three relaxation tests shown in Fig. 2 (Rubino et al., 2016). In the following, we use Eq. 2 and the set of oscillatory tests shown in Fig. 2 to compute the viscous shear stress in response to the strain state (ε_{ij}) associated with body waves (i.e., P- and S-waves) propagating at varying incidence angles and frequencies.

3. RESULTS

For the analysis of seismically-induced viscous shear stresses, we consider five cases defined by the properties given in Table 1. In addition to a reference scenario representative of a hard rock with brine saturating the fractures, we investigate four further scenarios where we modify (i) the fluid viscosity (case 2: water instead of brine saturating the fractures); (ii) the fracture aperture (case 3: wider fractures); (iii) the elastic moduli of the background medium (case 4: softer background medium); (iv) the length of the fractures (case 5: shorter fractures).

Property	Reference scenario	Modified scenario
Fluid viscosity η [Pa.s]	0.003	0.001 [Case 2]
Fluid bulk modulus K_f[GPa]	2.4	2.25 [Case 2]
Fracture aperture h [mm]	0.1	0.2 [Case 3]
Background bulk modulus K_b[GPa]	36.4	9 [Case 4]
Background shear modulus μ_b[GPa]	44	7 [Case 4]
Fracture length L [m]	0.36	0.28 [Case 5]

Table 1: Physical properties utilized for the sensitivity analysis of τ_{ij}.

In order to make the magnitude of τ_{xy} comparable for different directions of wave propagation, we assume that the strain associated with a seismic wave is the same for all incidence angles. The strain amplitudes are chosen based on the magnitude of the viscous shear stress that has been found to be sufficient to initiate fracture unclogging (Manga et al., 2012). Thus, for P-waves, we used a fixed extensional strain in the direction of wave propagation such that, for the reference scenario, the wave-induced τ_{xy} is ~0.1 Pa (e.g., for a 10 Hz P-wave, ε^{γ} ~1.5 x 10^{-7}, where the γ-axis coincides with the direction of wave propagation). Similarly, for the analysis of S-waves, we assume that the shear strain is the same regardless of the incidence angles and equal to the value used for P-waves.

We solve the numerical problem in the frequency domain and hence we obtain τ_{xy} as a function of the wave frequency ω. In the following, we present results in terms of $|\tau_{xy}(\omega)|$, which corresponds to the maximum of τ_{xy} during the oscillatory cycle at a given

position and at the frequency ω. In particular, we analyze the mean value of $|\tau_{xy}(\omega)|$ at the boundary between the fractures and the background, to have a representative value of the regions where unclogging is expected to take place. For brevity, we refer to this quantity as $\tau_{xy}(\omega)$.

3.1 Dependence of τ_{xy} on the seismic wave characteristics

Fig. 3 shows τ_{xy} as a function of incidence angle (0˚ to 90˚) and frequency (1, 10 and 100 Hz) in response to a strain state produced by plane P- (Fig. 3a) and S-waves (Fig. 3b). Fig. 3 shows that, as a consequence of the anisotropy of the fractured medium, the viscous shear stresses depends on the direction (θ) of the imposed seismic strain. For P-waves, maximal τ_{xy} is observed at θ=0˚ and θ=90˚. The reason is that at these angles the change in fluid pressure experienced by one fracture is much larger than that of the connected and less compressed fracture. The corresponding pressure gradient between the fractures produces the fluid motion that we observe in the form of strong τ_{xy}. On the other hand, the fracture distribution considered makes that at θ=45˚ both fractures are equally compressed by the P-wave and hence experience a similar fluid pressure increase. The lack of significant fluid pressure difference between horizontal and vertical fractures implies that there is no significant fluid pressure exchange and τ_{xy} becomes negligible (Fig. 3a). S-waves, on the other hand, show maximal τ_{xy} for θ=45˚ (Fig. 3b). In this case, the induced pressures have opposite signs in the horizontal and vertical fractures, respectively, which results in a large pressure gradient between them and maximal τ_{xy}. At θ=0˚ and θ=90˚, S-waves do not manage to increase fluid pressure inside the fractures and, correspondingly, τ_{xy} is negligible.

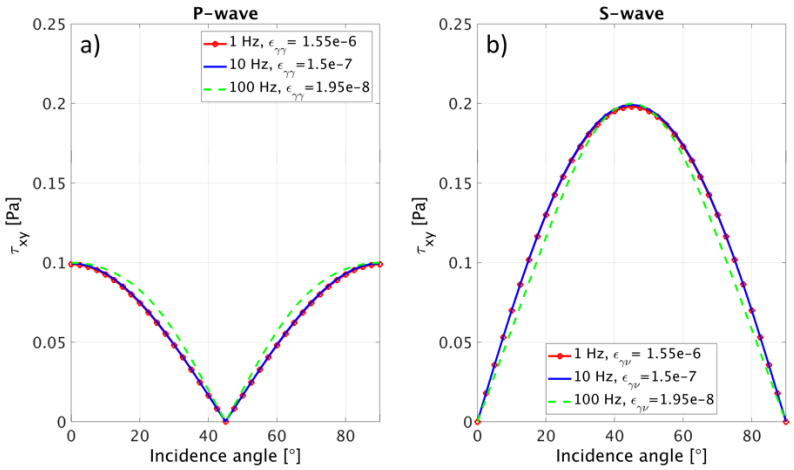

Figure 3: Seismically-induced τ_{xy} as a function of the incidence angle. Panels a) and b) show P- and S-waves, respectively. The physical properties correspond to those of the reference case in Table 1. For equal seismic strain values, the maximal τ_{xy} produced by S-waves is larger than the maximal τ_{xy} associated with P-waves. Note that the chosen strain magnitudes are in the range of typically observed values.

Comparison of the effects imposed by P- and S-waves in Fig. 3 suggests that S-waves can produce larger transient τ_{xy} for equal extensional and shear strain, respectively. Fig. 3 also shows the dependence of τ_{xy} with the magnitude of the seismic strain for P- and S-waves. We consider a frequency-dependent ε^{γ} such that, at each frequency considered, τ_{xy}=0.1 Pa at normal P-wave incidence. We observe that in order to obtain the same magnitude of τ_{xy}, a decrease in one order of magnitude in seismic wave frequency, requires an increase of approximately one order of magnitude in the seismic strain.

Lastly, Fig. 4 shows the dependence of τ_{xy} with the distance to the source. We assume that the seismic strain decays as 1/*r*, where *r* is the distance to the seismic source (Pride et al., 2008). We consider the same three frequencies as in Fig. 3 but the seismic strain at the source is assumed to be the same for all frequencies (ε^{γ}=1.55e-6). The viscous shear stress is computed at 0˚ and 45˚ for P- and S-waves, respectively, for which the effects are maximal due to the fracture distribution (Fig. 3). We observe that for typical seismic source strain magnitudes, τ_{xy} can be significantly above the threshold τ_{xy}=0.1 Pa. For frequencies characteristic of field experiments (tens of Hz), we can expect to initiate fracture unclogging even at tens of meters of distance from the source.

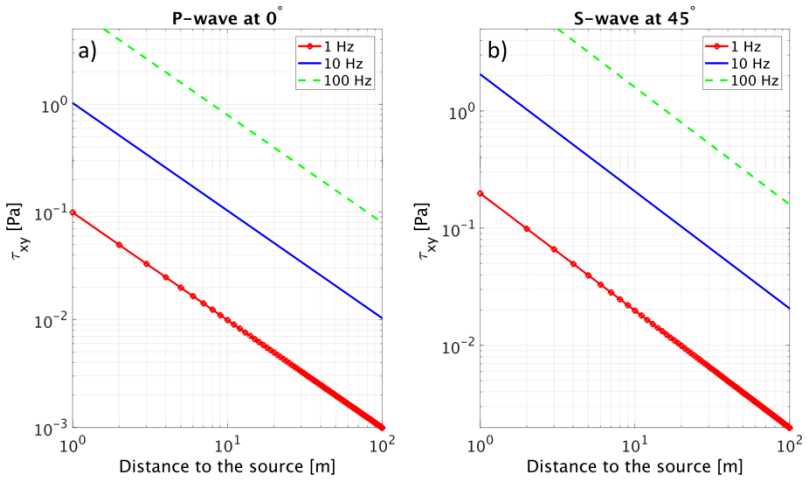

Figure 4: Seismically-induced τ_{xy} as a function of the distance to the seismic source. Panels a) and b) show the effects associated with P-waves at 0° and S-waves at 45°, respectively. The physical properties correspond to those of the reference case in Table 1. The decay of seismic strain amplitude is assumed to be frequency independent and inversely proportional to the distance to the seismic source.

3.2 Dependence of τ_{xy} on the physical properties of the fractured medium

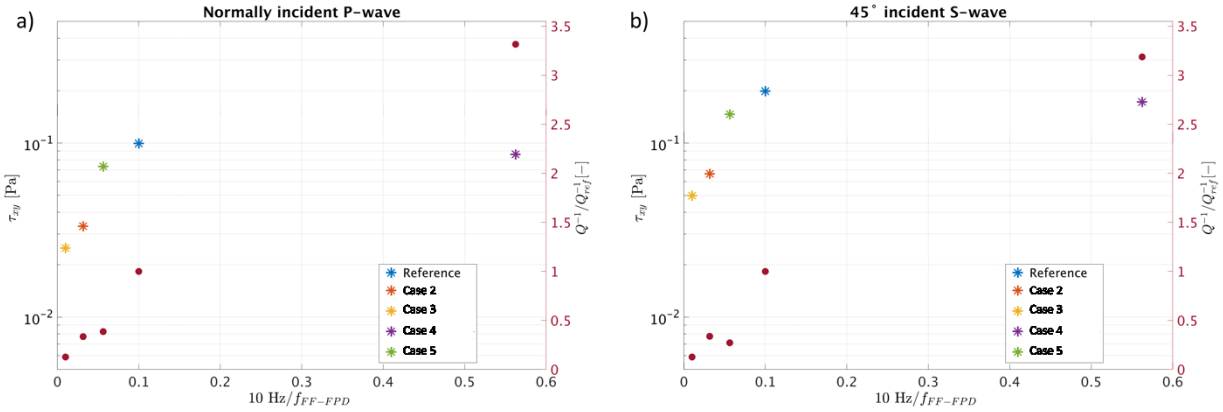

Figure 5: Seismically-induced τ_{xy} as a function of a normalized frequency (stars). Panels a) and b) show normally incident P-waves and 45 degrees incident S-waves, respectively. Red dots correspond to the ratio between the attenuation for each case and the attenuation of the reference scenario at 10 Hz. The REV properties for each case are described in Table 1.

The physical properties of the medium are expected to change the potential of fracture unclogging of a given formation subjected to given seismic stimulation conditions. Fig. 5 shows the changes in the magnitude of τ_{xy} for different fractured media whose properties are given in Table 1. We plot τ_{xy} for a single frequency equal to 10 Hz. The x-axis in Fig.5 corresponds to the ratio between the analyzed frequency (10 Hz) and the frequency at which the fluid pressure exchange between connected fractures during a half-cycle of the wave is maximum, leading to maximal seismic attenuation (f_{FF-FPD}) for each case (Fig. 5). This ratio provides an idea of how far the frequency of the seismic wave is from the optimal frequency of stimulation of the system as, in general, when the seismic wave frequency is close to f_{FF-FPD}, τ_{xy} is larger. For example, a fluid viscosity decrease from 0.003 Pa.s to 0.001 Pa.s (case 2) produces a decrease in τ_{xy} of ~70% at 10 Hz. Even larger changes in τ_{xy} occur when the aperture of the fractures is doubled with respect to the reference scenario. We also include in Fig. 4 the ratio between the seismic attenuation of each case and the attenuation of the reference scenario at 10 Hz. Note that the relative changes in seismic attenuation with respect to the reference scenario follow a similar trend as τ_{xy}. However, cases 4 and 5 show small departures from that correlation. By decreasing the aspect ratio of the fractures (Case 5), the attenuation does not increase as much as expected from the comparison with the other cases. This is due to the smaller fluid storage volume involved in the FPD process. On the other hand, the seismically-induced τ_{xy} is slightly larger than expected. In case 4, a background medium characterized by lower bulk and shear moduli compared with the reference scenario implies a decrease in f_{FF-FPD} resulting in a higher seismic attenuation. However, this does not translate into higher levels of τ_{xy} as shown in Fig. 5. Despite the fact that the relative changes in seismic attenuation are not always straightforwardly associated with the variations of τ_{xy}, they may provide an estimation of the relative potential of fracture unclogging of different regions of a reservoir.

3.3 Pressure and temperature dependence of τ_{xy}

In this section, we explore the influence of the fluid conditions on the development of viscous shear stresses in the fractures. To do so, we consider pure water as a geothermal fluid that is subjected to different pressures and temperatures. The water properties as a function of pressure and temperature are obtained from the International Association for Properties of Water and Steam Industrial

Formulation 1997 (IAPWS IF-97). We consider temperature values of 20, 300, 600, and 800˚C, and pressures of 1, 250, 500, and 1000 bars. For 20˚C and 300˚C the water is in liquid state while at 600˚C and 800˚C it is at supercritical state. For brevity, we only consider normally incident P-waves characterized by a frequency f=10 Hz and an extensional seismic strain of 4.5 x 10^{-7}. The latter is chosen in order to obtain τ_{xy}=0.1 Pa at close to ambient conditions (T=20˚C, P=1 bar).

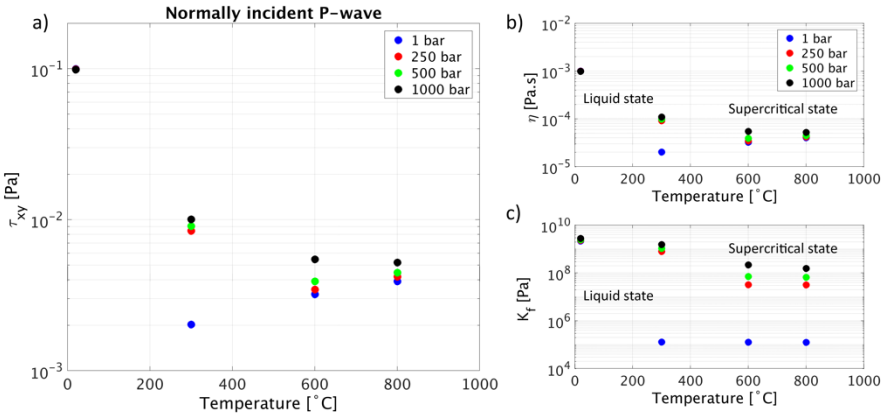

Figure 6: Seismically-induced τ_{xy} as a function of fluid temperature and pressure for a normally incident P-wave at f=10 Hz (panel a). We consider temperatures equal to 20, 300, 600, and 800 ˚C, and pressures of 1, 250, 500, and 1000 bar. The fluid viscosity and bulk modulus at the considered fluid temperatures and pressures are given in panels b and c, respectively. The imposed extensional seismic strain is 4.5 x 10^{-7}.

Fig. 6 shows that τ_{xy} is extremely dependent on the fluid pressure and temperature conditions. In liquid state, τ_{xy} decreases with temperature as both the viscosity and bulk modulus decrease as well (Fig. 6b and c). At 1000 bar, a change of temperature between 20˚C and 300˚C represents one order of magnitude decrease in τ_{xy}. Once supercritical state is reached, τ_{xy} starts to increase following the behavior of the viscosity and bulk modulus of the fluid. Overall, the pressure and temperature dependence of τ_{xy} is qualitatively similar to that of the fluid viscosity, which is also in agreement with Fig. 5.

The significant decrease of τ_{xy} with temperature for different pressures indicates that in order to maintain a certain value of τ_{xy}, it is necessary to increase the imposed seismic strain (or seismic frequency according to Fig. 3). In Fig. 7, we quantify the increase in seismic strain that is necessary to maintain τ_{xy}=0.1 Pa at all pressures and temperatures. As expected, the seismic strain follows the inverse relation with temperature and pressure compared with τ_{xy}. The largest increase corresponds to water in liquid state when temperature is increased from ambient conditions to 300˚C. In that case, the seismic strain imposed by the P-wave has to increase from 4.5 x10^{-7} to ~2 x10^{-5}. Although this represents an approximately two orders of magnitude increase, strains are still in the range of those typically observed for seismic waves.

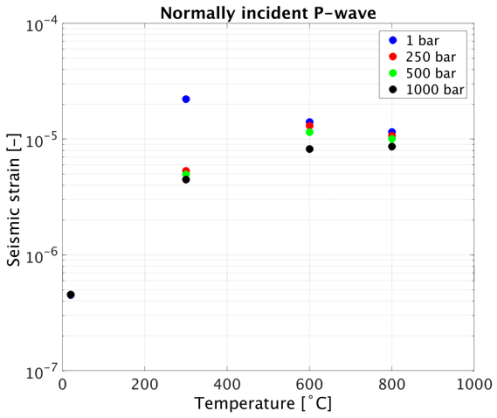

Figure 7: Seismic strain necessary to produce τ_{xy}=0.1 Pa for a normally incident P-wave as function of the fluid temperature and pressure. The fluid properties are the same as in Fig. 6.

3.4 Fracture geometry effect

The analysis performed utilizing 2D samples (Fig. 2) allowed us to examine the dependence of τ_{ij} on different seismic wave characteristics (i.e., strain, frequency, direction of propagation), fractured rock (e.g., host rock stiffness, fracture aspect ratio), and fluid properties (e.g., fluid viscosity). However, the 2D nature of the simulations prevent us from modelling the effects associated with a spatially heterogeneous distribution of properties along the fracture plane. In particular, local variations in fracture aperture cannot be modelled with 2D numerical samples. In order to study the effects of fracture aperture distribution, here we consider the 3D sample shown in Fig. 8. For brevity we only consider normal P-wave incidence, which means that we subject the sample to an undrained oscillatory relaxation test in which a normal displacement is applied along the top surface of the sample, while the lateral

and bottom surfaces are confined. We allow the fracture aperture (h) to be equal to 1 mm (open fracture regions filled with fluid) or 0 mm (fracture walls in contact represented with background rock properties). The corresponding fluid and elastic background physical properties are those given in Table 1 for the reference scenario. The 3D sample contains two orthogonal fractures, whose aperture distribution is the same (Fig. 8). The aperture distribution of the fractures was generated using the stratified percolation approach of Nolte and Pyrak-Nolte (1991). For computational reasons, we have considered an open fracture aperture 10 times larger than for the 2D samples shown in Fig. 2. Given that for thicker fractures f_{FF-FPD} increases (Fig. 5), we impose a seismic strain of ε^{Y}=2 x10^{-5} to have viscous shear stress values above 0.1 Pa for all the analyzed cases.

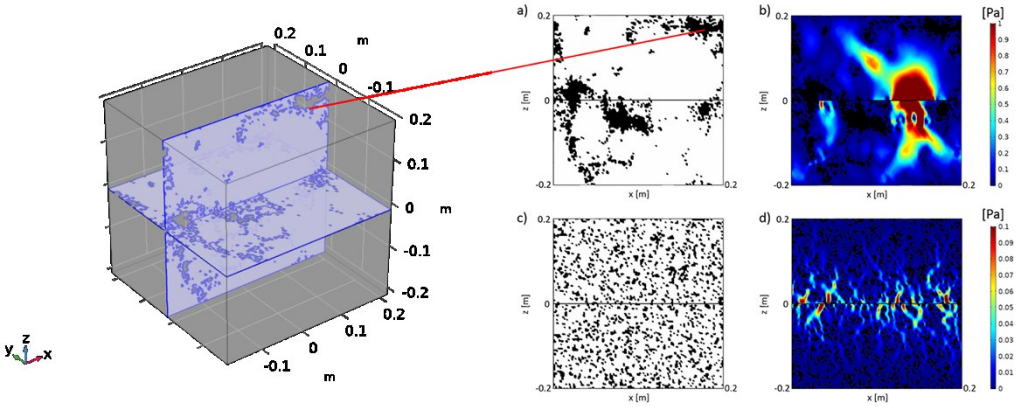

Figure 8: Fracture geometry (a and c) and τ_{yz} for f=10 Hz and P-wave incidence (b and d). The synthetic sample on the left represents a unit cell of a 3D periodically fractured rock. The sample illustrates the case of two connected orthogonal fluid-saturated fractures with the contact area geometry shown in panel a. The plots are computed at one of the interfaces between each fracture and the background. Black and white regions in a and c illustrate contact areas and open fracture, respectively. Panels a and c correspond to fractures with same volume but longer and shorter contact area lengths, respectively. Note the different color scales in panels b and d.

We first consider the case of two fractures with equal contact area density (10%) but exhibiting long and short characteristic lengths of the contact areas (black regions in Fig. 8a and c, respectively). Figs. 8b and d show the component of the viscous shear stress tensor τ_{yz} in the vertical fracture, which is the most affected by FPD between fractures since both fractures are perpendicular to the yz-plane. Cold and hot colours in Fig. 8 denote low and high τ_{yz}, respectively, while contact areas are plotted in black. Large values of τ_{yz} can only be present in the open fracture regions. Due to the spatial distribution of the contact areas, the fracture with longer contact areas tends to be mechanically more compliant than the one with smaller contact areas. The corresponding larger compressibility contrast with respect to the background results in larger τ_{yz} in the case of the fracture with longer contact areas (Fig. 8b) compared with that shown in Fig. 8d.

In order to minimize the effect of mechanical compliance of the fracture, we consider three more fractures which have different contact area density and characteristic length but exhibit similar mechanical compliance. Fig. 9 shows the volumetric average of τ_{yz} in the fractures per unit of fracture volume for 4 fracture cases having different contact area density but similar mechanical compliance. The mechanical compliance affects the P-wave modulus, which is shown in the right panel of Fig. 9 and their similarity implies that the 4 fracture distributions yield comparable seismic responses. However, the ability of seismic waves to induce large viscous shearing is not the same for all fractures. As shown in the left panel of Fig. 9, as the contact area density increases in fractures of similar mechanical compliance, the seismically-induced viscous shearing tends to increase as well. This is due to the fact that higher contact area density imply larger open regions, which, as illustrated in Fig. 8b, allow for more viscous shearing.

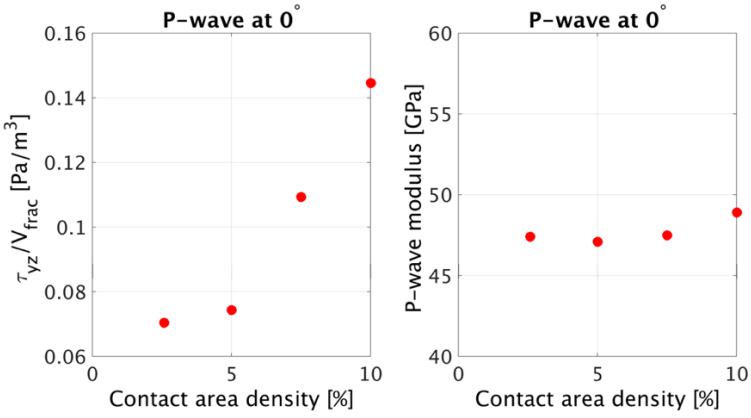

Figure 9: τ_{yz} per unit of volume fracture as a function of contact area density for f=10 Hz and P-wave normal incidence (left). We consider fractures with similar mechanical compliances, which implies that the effective P-wave modulus of the fractured medium under dry conditions is approximately constant (right). To obtain similar fracture mechanical compliances, we increase the contact area correlation length as the contact area density increases.

4. CONCLUSIONS

Numerical simulations of seismically-induced viscous shearing in the fluid saturating a system of fractures show that fracture unclogging is plausible for strain magnitudes and frequencies typically used in field and laboratory measurements. For a system of orthogonally intersecting fractures, the development of viscous shear stress depends not only on the frequency and seismic strain magnitude but also on the direction of wave propagation. Moreover, this anisotropic effect is not the same for all wave modes. For example, viscous shearing for P- and S-wave is at its minimum and maximum, respectively, at 45˚ incidence angle. Interestingly, for the same magnitude of seismic strain, the viscous shearing produced by S-waves was found to be approximately two times larger than the maximal effects of P-waves.

Regarding the influence of the physical properties of the medium, larger viscous shear stress is expected for more viscous fluids, stiffer background rocks, and thinner fractures. The development of strong viscous shearing is controlled by the ratio f/f_{FF-FPD} where f is the seismic wave frequency and f_{FF-FPD} is the frequency at which the fluid pressure gradient between the more compressed fracture and the connected (and less compressed) fracture produces maximal seismic attenuation. Given that f_{FF-FPD} depends on the physical properties of the fractured medium, this implies that regions where pore fluids change or with different pressure and temperature conditions may experience more fracture unclogging, and consequently stronger permeability enhancement, than others. Finally, we found that the fracture aperture distribution also controls the development of viscous shear stresses. Spatially heterogeneous fracture apertures can produce locally enhanced viscous shearing, which tend to be more pronounced when the characteristic size of the open regions of the fracture increases.

Although our results suggest that dynamically changing permeability of fractured systems may be feasible, artificial stimulation of reservoirs represent an engineering challenge. Applying enhanced oil recovery technologies to fractured environments seems to be a first step towards the development of suitable technologies in this kind of environments. Our analysis points out the role of the seismic wave frequency, mode, directivity, and imposed strain on the potential of fracture unclogging in a fractured formation. Future research should be focused on studying additional factors, such as stimulation duration and reservoir structure, which are also expected to influence the magnitude of the seismically-induced viscous shearing. The methodology used in this work to obtain the viscous shear stress inside an REV of a given formation of interest due to an arbitrary strain state can help to find the corresponding set up optimization.

REFERENCES

Ameli, P., Elkhoury, J. E., Morris, J. P., and Detwiler, R. L.: Fracture permeability alteration due to chemical and mechanical processes: a coupled high-resolution model. *Rock mechanics and rock engineering*, **47**, (2014), 1563-1573.

Bai, R., and Tien, C.: Particle detachment in deep bed filtration. *Journal of colloid and interface science*, **186**, (1997), 307-317.

Beresnev, I. A., and Johnson, P. A.: Elastic-wave stimulation of oil production: A review of methods and results. *Geophysics* , **59**, **(**1994), 1000-1017.

Bergendahl, J., and Grasso, D.: Prediction of colloid detachment in a model porous media: Hydrodynamics. *Chemical Engineering Science* , **55**, (2000), 1523-1532.

Borg, I., Stone, R., Levy, H., and Ramspott, L.: Information pertinent to the migration of radionuclides in ground water at the Nevada test site. part 1. review and analysis of existing information (*Technical Report*). California Univ. (1976).

Brodsky, E. E., Roeloffs, E., Woodcock, D., Gall, I., and Manga, M.: A mechanism for sustained groundwater pressure changes induced by distant earthquakes. *Journal of Geophysical Research: Solid Earth*, **108**, (2003).

Brodsky, E. E., and Prejean, S. G.: New constraints on mechanisms of remotely triggered seismicity at long valley caldera. *Journal of Geophysical Research: Solid Earth* , **110**, (2005).

Economides, M. J., and Nolte, K. G.: Reservoir stimulation (Vol. 2). Prentice Hall Englewood Cliffs, NJ. (1989).

Elkhoury, J. E., Brodsky, E. E., and Agnew, D. C.: Seismic waves increase permeability. *Nature* , **441**, (2006), 1135.

Elkhoury, J. E., Niemeijer, A., Brodsky, E. E., and Marone, C.: Laboratory observations of permeability enhancement by fluid pressure oscillation of in situ fractured rock. *Journal of Geophysical Research: Solid Earth*, **116**, (2011).

Farías, C., Lupi, M., Fuchs, F., and Miller, S. A.: Seismic activity of the Nevados de Chillán volcanic complex after the 2010 Mw8.8 Maule, Chile, earthquake. *Journal of Volcanology and Geothermal Research*, **283**, (2014), 116-126.

Kocharyan, G., Vinogradov, E., Gorbunova, E., Markov, V., Markov, D., and Pernik, L.: Hydrologic response of underground reservoirs to seismic vibrations. *Izvestiya, Physics of the Solid Earth*, **47**, (2011), 1071-1082.

Kutay, M. E., and Aydilek, A. H.: Pore pressure and viscous shear stress distribution due to water flow within asphalt pore structure. *Computer-Aided Civil and Infrastructure Engineering*, **24**, (2009), 212-224.

Li, X., Zhang, P., Lin, C., and Johnson, W. P.: Role of hydrodynamic drag on microsphere deposition and re-entrainment in porous media under unfavorable conditions. *Environmental science & technology*, **39**, (2005), 4012-4020.

Lupi, M., Saenger, E. H., Fuchs, F., and Miller, S.: Lusi mud eruption triggered by geometric focusing of seismic waves. *Nature Geoscience*, **6**, (2013), 642.

Lupi, M., Ricci, B. S., Kenkel, J., Ricci, T., Fuchs, F., Miller, S. A., and Kemna, A.: Subsurface fluid distribution and possible seismic precursory signal at the Salse di Nirano mud volcanic field, Italy. *Geophysical Journal International*, **204**, (2015), 907-917.

Lupi, M., Frehner, M., Weis, P., Skelton, A., Saenger, E. H., Tisato, N., . . . Driesner, T.: Regional earthquakes followed by delayed ground uplifts at campi Flegrei caldera, Italy: Arguments for a causal link. *Earth and Planetary Science Letters*, **474**, (2017), 436-446.

Lupi, M., Fuchs, F., and Saenger, E. H.: Numerical simulations of passing seismic waves at the Larderello-Travale geothermal field, Italy. *Geophysical Research Letters*, **44**, (2017), 5418-5426.

Manga, M., Brodsky, E. E., and Boone, M.: Response of stream flow to multiple earthquakes. *Geophysical Research Letters* , **30**, (2003).

Manga, M., and Brodsky, E.: Seismic triggering of eruptions in the far field: Volcanoes and geysers. *Annu. Rev. Earth Planet. Sci*, **34**, (2006), 263-291.

Manga, M., Beresnev, I., Brodsky, E. E., Elkhoury, J. E., Elsworth, D., Ingebritsen, S. E., . . . Wang, C.-Y.: Changes in permeability caused by transient stresses: Field observations, experiments, and mechanisms. *Reviews of geophysics*, **50**, (2012). 28.

Mirzaei-Paiaman, A., and Nourani, M.: Positive effect of earthquake waves on well productivity: Case study: Iranian carbonate gas condensate reservoir. *Scientia Iranica*, **19**, (2012), 1601-1607.

Mogi, K., Mochizuki, H., and Kurokawa, Y.: Temperature changes in an artesian spring at Usami in the Izu peninsula (Japan) and their relation to earthquakes. *Tectonophysics*, **159**, (1989), 95-108.

Nolte, D., and Pyrak-Nolte, L.: Stratified continuum percolation: Scaling geometry of hierarchical cascades. *Physical Review A*, **44**, (1991), 6320.

Pride, S. R., Flekkøy, E. G., and Aursjø, O.: Seismic stimulation for enhanced oil recovery. *Geophysics*, **73**(5), (2008), O23–O35.

Pyrak-Nolte, L. J., and Nolte, D. D.: Approaching a universal scaling relationship between fracture stiffness and fluid flow. *Nature communications*, **7**, (2016), 10663.

Quintal, B., Rubino, J. G., Caspari, E., and Holliger, K.: A simple hydromechanical approach for simulating squirt-type flow. *Geophysics*, **81**, (2016), D335-D344.

Rojstaczer, S., Wolf, S., and Michel, R.: Permeability enhancement in the shallow crust as a cause of earthquake-induced hydrological changes. *Nature*, **373**, (1995), 237.

Rubino, J. G., Guarracino, L., Müller, T. M., and Holliger, K.: Do seismic waves sense fracture connectivity?. *Geophysical Research Letters*, **40**, (2013), 692-696.

Rubino, J. G., Caspari, E., Müller, T. M., Milani, M., Barbosa, N. D., and Holliger, K.: Numerical upscaling in 2-d heterogeneous poroelastic rocks: Anisotropic attenuation and dispersion of seismic waves. *Journal of Geophysical Research: Solid Earth*, **121**, (2016), 6698-6721.

Rudolph, M., and Manga, M.: Mud volcano response to the 4 april 2010 El Mayor-Cucapah earthquake. *Journal of Geophysical Research: Solid Earth*, **115**, (2010).

Wang, C.-Y.: Liquefaction beyond the near field. *Seismological Research Letters*, **78**, (2007), 512-517.

Xue, L., Li, H.-B., Brodsky, E. E., Xu, Z.-Q., Kano, Y., Wang, H., . . . Zhang, W.: Continuous permeability measurements record healing inside the Wenchuan earthquake fault zone. *Science*, **340**, (2013), 1555-1559.

Zhang, Y., Fu, L.-Y., Huang, F., and Chen, X.: Coseismic water-level changes in a well induced by teleseismic waves from three large earthquakes. *Tectonophysics*, **651**, (2015), 232-241.